NANO LETTERS

Letter

pubs.acs.org/NanoLett

Magnetic Skyrmion Formation at Lattice Defects and Grain Boundaries Studied by Quantitative Off-Axis Electron Holography

Zi-An Li,[*,†,‡,§] Fengshan Zheng,[‡] Amir Hossein Tavabi,[‡] Jan Caron,[‡] Chiming Jin,[⊥] Haifeng Du,[⊥] András Kovács,[‡] Mingliang Tian,[⊥] Michael Farle,[†,∥] and Rafal E. Dunin-Borkowski[‡]

[†]Faculty of Physics and Center for Nanointegration (CENIDE), University of Duisburg-Essen, 47057 Duisburg, Germany

[‡]Ernst Ruska-Centre for Microscopy and Spectroscopy with Electrons and Peter Grünberg Institute, Forschungszentrum Jülich, 52425 Jülich, Germany

[§]Institute of Physics, Chinese Academy of Sciences, 100190 Beijing, China

[⊥]High Magnetic Field Laboratory, Chinese Academy of Sciences, 230031 Anhui, China

[∥]Center for Functionalized Magnetic Materials (FunMagMa), Immanuel Kant Baltic Federal University, Kaliningrad, Russian Federation

S *Supporting Information*

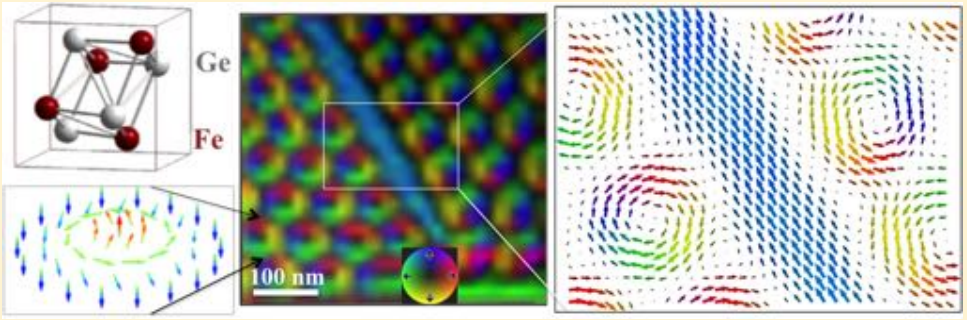

ABSTRACT: We use in situ Lorentz microscopy and off-axis electron holography to investigate the formation and characteristics of skyrmion lattice defects and their relationship to the underlying crystallographic structure of a B20 FeGe thin film. We obtain experimental measurements of spin configurations at grain boundaries, which reveal inversions of crystallographic and magnetic chirality across adjacent grains, resulting in the formation of interface spin stripes at the grain boundaries. In the absence of material defects, we observe that skyrmions lattices possess dislocations and domain boundaries, in analogy to atomic crystals. Moreover, the distorted skyrmions can flexibly change their size and shape to accommodate local geometry, especially at sites of dislocations in the skyrmion lattice. Our findings provide a detailed understanding of the elasticity of topologically protected skyrmions and their correlation with underlying material defects.

KEYWORDS: *Magnetic skyrmion, off-axis electron holography, Lorentz microscopy, FeGe helimagnet, magnetic defects*

Magnetic skyrmions are particle-like topologically protected swirling spin textures.[1] Their nanoscale size,[1] topologically protected stability,[2] and efficient coupling to spin-polarized currents[3,4] make them promising magnetic elements for data storage and spintronic device applications.[5] Chiral-type magnetic skyrmions are stabilized by the Dzyaloshinskii–Moriya (DM) interaction,[6,7] which is associated with broken inversion symmetry and spin–orbit coupling. In the presence of a specific magnetic field and over a well-defined temperature range, DM-stabilized chiral skyrmions tend to crystallize into ordered skyrmion lattices.[8,9] However, in analogy to atoms in a crystal lattice, particle-like skyrmion spin textures are expected to form not only perfect skyrmion lattices, but also lattices that contain defects.[9,10] For both fundamental research and practical applications, it is important to develop a full understanding of the formation and characteristics of skyrmion defects and their relationship to the crystallography of underlying atomic lattices. Key questions relate to (1) the relationship between skyrmion lattice defects, crystallographic defects, and structural chirality; (2) the influence of grain boundaries on skyrmion chirality, nucleation, and lattice structure; and (3) the formation and characteristics of skyrmion lattice defects in perfect defect-free single crystals.

To address these questions, direct imaging of magnetic skyrmions with nanometer spatial resolution is essential. A plethora of advanced magnetic imaging techniques has been applied to image magnetic skyrmions, including spin-polarized scanning tunnelling microscopy (SP-STM),[11] X-ray magnetic circular dichroism in scanning transmission X-ray microscopy

Received: October 12, 2016
Revised: December 26, 2016
Published: January 26, 2017

DOI: 10.1021/acs.nanolett.6b04280
Nano Lett. 2017, 17, 1395–1401

(XMCD-STXM),[12] and magnetic force microscopy (MFM).[13] However, STXM and MFM are not suited to resolving the fine internal spin textures of skyrmions due to their relatively poor spatial resolutions (a few tens of nanometers). SP-STM has stringent requirements for clean material surfaces and is limited to the observation of spin structure at surfaces. On the other hand, several techniques based on transmission electron microscopy (TEM) have been used to image magnetic skyrmions, including Lorentz microscopy (LM),[9,14] off-axis electron holography (EH),[15,16] and differential phase contrast (DPC) imaging.[17,18] These real-space imaging techniques allow direct visualization and quantification of the spin textures of skyrmion lattices and defects. They have been used to study ordered skyrmion lattices in extended thin films of several B20-type chiral magnets. Examples include studies of MnSi,[19] FeGe,[10] $Fe_{1-x}Co_xSi$,[9] and $Fe_{1-x}Ge_xSi$.[20] Skyrmions in chiral magnets have been found to support not only ordered structures, but also lattices with topological defects such as magnetic twins,[14] domain boundaries,[10] and dislocations.[20] Recently, the formation of skyrmion grain boundaries in $FeGe_{1-x}Si_x$[21] and the effect of applied magnetic field and film thickness on the formation of skyrmion grain boundaries in MnSi were reported.[22] Despite the fact that skyrmion defects were investigated in these studies, their spin configurations were not quantitatively determined, in part due to limited spatial resolution and the difficulty of quantifying spin structures from magnetic contrast on an absolute scale.[23] We also point out that in light of local magnetic structure analysis around the sample interfaces or edges, off-axis EH has advantages over the LM method combined with magnetic transport-of-intensity equation (TIE) analysis. A recent example of magnetic induction mapping at the edges of FeGe specimens using LM-TIE still contained artifacts even though interfacial Fresnel fringes were significantly reduced due to the presence of extra layers at the specimen edge.[24]

Here, we combine in situ LM and quantitative off-axis EH to investigate the formation of magnetic skyrmion lattices in B20-type FeGe thin films. We correlate magnetic skyrmion lattice defects with the underlying crystallography of the material and show that the crystallographic nature of a grain boundary has a profound influence on the nucleation and chirality of an associated magnetic skyrmion lattice. Furthermore, we quantitatively determine the in-plane projected magnetization associated with skyrmion lattice defects.

Experiment. Noncentrosymmetric B20 FeGe, a prototype chiral magnet with a Curie temperature of ~278 K, was prepared in the form of a thin lamella using focused ion beam (FIB) milling and a lift-out method. Details of both specimen preparation and preliminary structural characterization using an FEI F20 microscope operated at 200 kV are given in the Supporting Information. For magnetic imaging, we used an image-aberration-corrected FEI Titan 80−300 microscope equipped with a Lorentz lens and two electron biprisms. The use of a liquid nitrogen-cooled specimen holder (Gatan, Inc.) allowed the sample temperature to be varied between 95 and 370 K. The objective lens of the microscope was used to apply out-of-plane magnetic fields of between 0 and 1.5 T. In situ LM was carried out as a function of temperature and applied magnetic field. Off-axis EH measurements were conducted to obtain quantitative magnetic phase images of the spin structures of skyrmion defects.

Results and Discussion. *Expected Behavior of Skyrmion Lattice Defects.* In a single crystal, crystallographic chirality describes the situation when a distribution of atoms cannot be brought into coincidence with its mirror image by applying any combination of rotations and translations.[25] Usually, the space group must not contain inversion, rotation-inversion, or mirror planes. This criterion is satisfied by the noncentrosymmetric B20 crystallographic structure[26,27] (space group $P2_13$, no. 198). The atoms in a B20 structure are assembled in the 4*a* Wyckoff positions $R_1(\mu, \mu, \mu)$, $R_2(0.5+\mu, 0.5-\mu, -\mu)$, $R_3(-\mu, 0.5+\mu, 0.5-\mu)$, and $R_4(0.5-\mu, -\mu, 0.5+\mu)$. In FeGe, according to the International Tables for Crystallography,[28] μ^RGe = 0.154 and μ^RFe = 0.865 for the right-handed structure, whereas μ^LGe = 0.846 and μ^LFe = 0.135 for the left-handed structure. In homogeneous B20-type helimagnets that possess a bulk DM interaction, magnetic chirality Γ_M is inherited from the underlying crystallographic chirality Γ_C,[29,30] where $\Gamma_M = \alpha \times \Gamma_C$, and α is the sign of the DM interaction. Figure 1a shows a schematic illustration of the relationship between crystallographic and magnetic chirality.

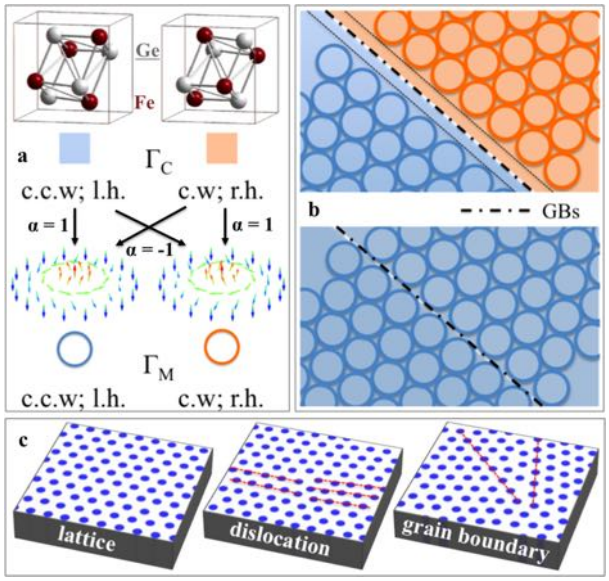

Figure 1. Schematic representations of magnetic skyrmion lattice defects mediated by underlying crystallographic defects. (a) The senses of rotation of crystal chirality Γ_C and magnetic chirality Γ_M, denoted either by a counterclockwise (c.c.w.) or a left-handed (l.h.) character, or by a clockwise (c.w.) or a right-handed (r.h.) character. Colored circles and squares denote the magnetic and crystal chirality, respectively. (b) Grains with and without reversed crystallographic (magnetic) chirality across a grain boundary (GB). Circles of different color denote skyrmions of different chirality. (c) Formation of magnetic skyrmion defects in the absence of material defects.

In the present study, we examine two FeGe specimens that contain crystallographic grain boundaries, as shown schematically in Figure 1b. In the first specimen, the crystallographic chirality of the grains is reversed across the boundary, as shown in the upper panel of Figure 1b. In the second specimen, the crystallographic chirality is unchanged across the grain boundary, as shown in the lower panel of Figure 1b. It is expected that the magnetic skyrmion arrangements across the grain boundaries will be distinctly different in the two specimens. For the case of reversed chirality, a stripe-like region of magnetization is expected to form at the grain boundary. The formation of such spin stripes across grains of reversed chiralities preserves magnetic chirality at both grains

DOI: 10.1021/acs.nanolett.6b04280
Nano Lett. 2017, 17, 1395−1401

and meets the requirement of minimum magnetostatic energy.[31] The same argument applies to the grains of identical chirality, in which skyrmions are expected to pack closely at the grain boundary, as illustrated in Figure 1b.

In a single crystal, in the absence of crystallographic pinning sites, skyrmion lattices are also expected to support defects such as dislocations[17] and domain boundaries.[21,32] Figure 1c schematically illustrates the formation of a dislocation, and a domain boundary in a skyrmion lattice in a single crystal helimagnet.

Lorentz Microscopy of Grain Boundaries. Over a certain range of applied magnetic field and temperature, the spins of Bloch-type magnetic skyrmions typically have a fixed helicity that is either counterclockwise (c.c.w.) or clockwise (c.w.). Such noncollinear spin textures can be visualized readily using LM by recording a Fresnel (defocus) image.[33] The deflection of the electron beam by the magnetic fields of individual skyrmions is then captured in the form of bright and dark contrast centered on the position of each skyrmion.

To examine the effect of underlying crystallographic defects on skyrmion lattice formation, we examined two lamellae, whose microstructures are detailed in the Supporting Information. Examination of the two specimens allows an assessment of whether grain boundaries facilitate or suppress skyrmion nucleation in the presence of applied fields. In this regard, we recorded the field- and temperature-dependent magnetization evolution of the two FeGe lamella using LM, as shown in the Supporting Information. Careful inspection of the results from the videos reveals that, during the helix-to-skyrmion transition, skyrmion nucleation depends strongly on the orientation of a helix relative to that of a grain boundary. The orientation of spin helix is characterized by the propagation direction of the helical spin configurations, so-called helix propagation vector q, as seen in Figure 2a. When the helix propagation vector is oriented parallel to a grain boundary, skyrmions appear to nucleate readily in the grain boundary region. In contrast, skyrmion formation is suppressed at a grain boundary region that is perpendicular to the helix propagation vector, as seen in Figure 2b. We therefore suggest that the orientation of helices relative to a grain boundary, rather than the simple presence of a grain boundary region, is critical for skyrmion nucleation. Such grain-boundary-mediated skyrmion formation is similar to edge-mediated skyrmion formation, which was reported recently in a FIB-prepared FeGe nanostripe,[24] in which the helix orientation relative to the edge played a decisive role.

Figure 3 shows under focused (−400 μm) LM images of the two specimens recorded at 220 K in an applied out-of-plane field of 100 mT. The round contrast features correspond to individual magnetic skyrmions, while the pairs of white arrows mark the positions of crystallographic grain boundaries. In Figure 3a, a reversal in skyrmion contrast across the grain boundary is associated with a reversal in the magnetic chirality of the skyrmions. In comparison, the skyrmion contrast is unchanged across the grain boundary shown in Figure 3b. This difference is associated with the fact that the grains in Figure 3a possess reversed crystallographic chirality, while the grains in Figure 3b possess identical crystallographic chirality. Careful inspection of the magnetic contrast at the grain boundary in Figure 3a reveals stripe-like contrast with a width of approximately one skyrmion, while such contrast is absent from Figure 3b. In both cases, the skyrmions form a triangular lattice within each grain, and no skyrmions form at the grain boundaries. This behavior is associated with the role of the interfaces themselves in the nucleation of skyrmions from magnetic helices, as discussed above.

Although LM allows direct visualization of magnetic structures, the indirect relationship between the recorded Fresnel contrast and the magnetic structure makes quantitative determination of the local magnetization extremely difficult. In

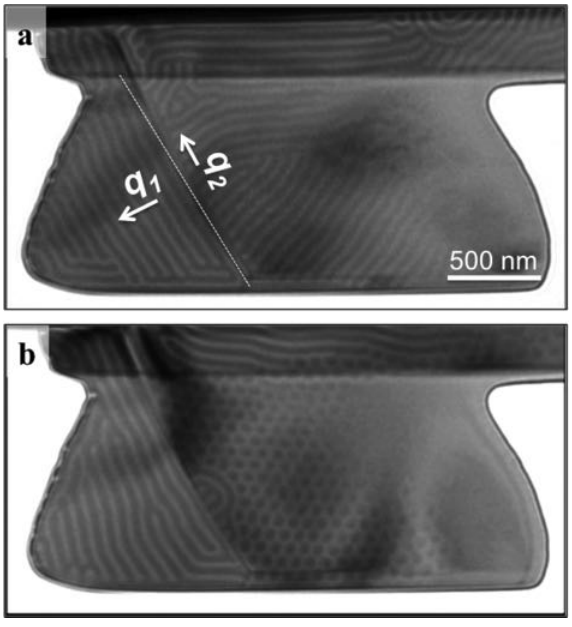

Figure 2. Lorentz microscopy of an FIB-prepared FeGe lamella, showing (a) magnetic helices under zero field and (b) skyrmions under 100 mT at 220 K in a region with reversed crystallographic (magnetic) chirality across crystallographic grain boundaries. The helical propagation vectors q_1 and q_2 are indicated by arrows.

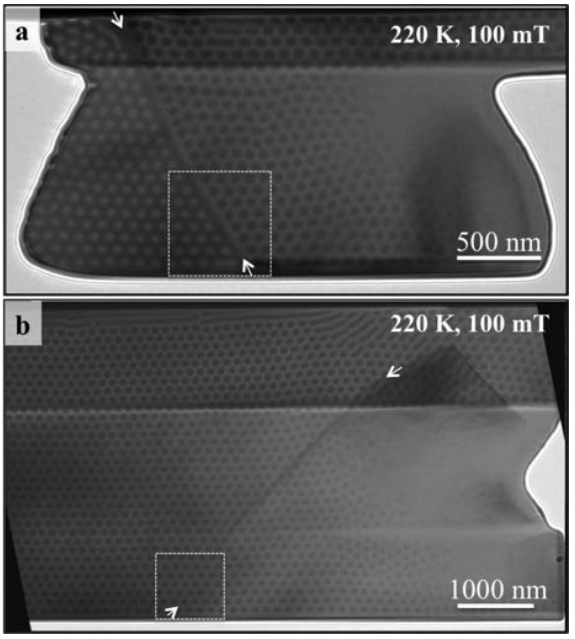

Figure 3. Lorentz microscopy of FIB-prepared FeGe lamella, showing skyrmion lattices formed (a) with and (b) without reversed crystallographic (magnetic) chirality across crystallographic grain boundaries. See text for details.

DOI: 10.1021/acs.nanolett.6b04280
Nano Lett. 2017, 17, 1395−1401

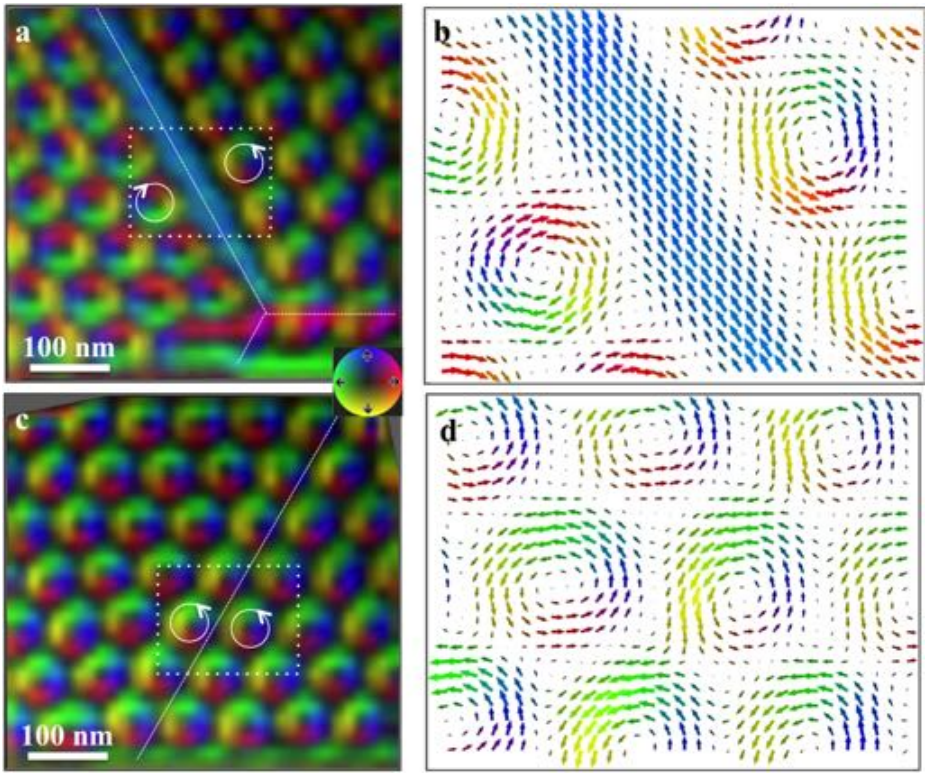

Figure 4. Spin textures of magnetic skyrmions at crystallographic grain boundaries measured using off-axis electron holography. (a) Color-contour composite image derived from a magnetic phase image of the FeGe lamella shown in Figure 3a. (b) Projected in-plane magnetization reconstructed from the magnetic phase image used to generate panel a. (c) Color-contour composite image derived from a magnetic phase image of the FeGe lamella shown in Figure 3b. (d) Projected in-plane magnetization reconstructed from the magnetic phase image used to generate panel c. The hue and brightness in panels a and c represent the direction and magnitude of the projected in-plane magnetic induction, respectively. The phase contour lines have a spacing of $2\pi/100$ radians. The circular contrast features correspond to individual magnetic skyrmions. The white dashed lines in panels a and c denote the crystallographic grain boundaries.

contrast, the TEM mode of off-axis EH allows the phase change of the high-energy electron waves that has traversed a specimen to be recorded directly.[34] The obtained phase information can then be used to determine the projected in-plane magnetic field within and around the specimen quantitatively.[15]

Off-Axis Electron Holography of Grain Boundaries. The examination of spin textures at crystallographic grain boundaries using EH through the quantitative analysis of phase images requires the separation of the magnetic signal of interest from the effects of local variations in mean inner potential and specimen thickness. The approach that was used to achieve this separation here is described in the Supporting Information. Figure 4a shows a resulting color-contour composite image determined from a magnetic phase image recorded using EH from the area marked in Figure 3a. The hue and brightness of the colors denote the direction and magnitude of the projected in-plane magnetic induction, respectively. The spacing of the contour lines is related directly to the magnitude of the in-plane magnetization integrated in the electron beam direction. The dashed lines mark the positions of crystallographic grain boundaries. The magnetic induction map confirms that the sense of spin rotation of the skyrmions changes across the grain boundary. Strikingly, a spin stripe is clearly observed along the grain boundary itself. The width of the spin stripe is estimated to be ~65 nm, which is close to the typical helical pitch L_D of 70 nm for FeGe.[35] To reconstruct the spin structure from the recorded magnetic phase image quantitatively, we employed a model-based iterative magnetization reconstruction technique. The principle and practical details of the iterative algorithm are provided in the Supporting Information. Figure 4b shows the reconstructed projected in-plane magnetization distribution of the region outlined in Figure 4a. The arrows denote the direction and magnitude of the reconstructed local projected in-plane magnetization. For the purpose of clear representation, only one-fifth of the reconstructed spins are plotted. Although the spin stripe at the grain boundary was observed using LM previously, its spin texture was not determined. Here, our magnetization reconstruction technique, applied to a holographic magnetic phase image, allows the precise local spin texture to be quantified. Although the underlying structural boundary is atomically sharp, the skyrmion domain boundary is characterized by a spin stripe, whose width is on the order of one characteristic chiral length L_D. Such a spin stripe preserves the magnetic chirality on each side of the boundary during skyrmion formation and is reminiscent of edge spin states at a specimen edge.[24,31]

In contrast, when the adjacent grains have identical crystallographic chirality (lower panel in Figure 4b), the skyrmions in both grains have identical senses of rotation, as shown in the form of a color-contour image in Figure 4c. No stripe-like spin textures are present in the grain boundary region, which is in marked contrast to the situation for grains of reversed chirality. Figure 4d shows the corresponding reconstructed magnetization distribution in the region outlined in Figure 4c. Careful inspection of the reconstructed magnet-

DOI: 10.1021/acs.nanolett.6b04280
Nano Lett. 2017, 17, 1395−1401

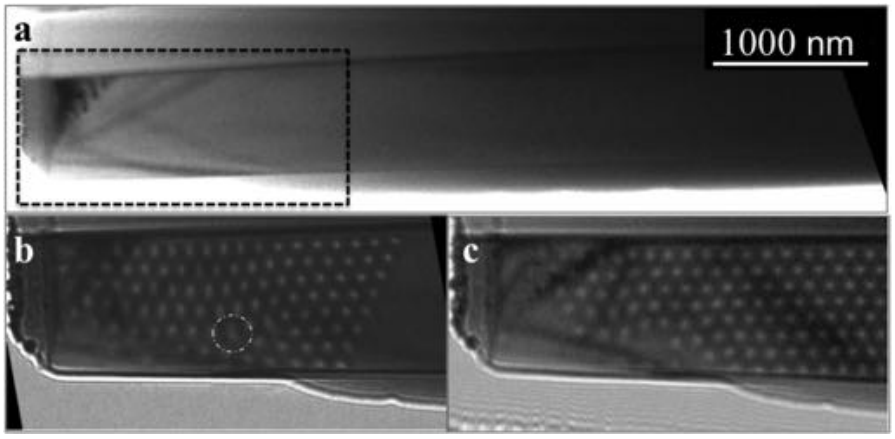

Figure 5. Lorentz microscopy of a skyrmion lattice dislocation in an FeGe nanostripe. (a) Bright-field TEM image of an FeGe nanostripe in a thickness wedge. The dashed area was used for LM studies. (b, c) Lorentz micrographs (recorded at a defocus of −400 μm) of a skyrmion lattice with and without a dislocation, respectively. The specimen was cooled at 100 K and imaged in an applied filed of 100 mT. Note that the cooling rate for panel b is about 10 K min^{-1}, while for panel c it is about 1 K min^{-1}.

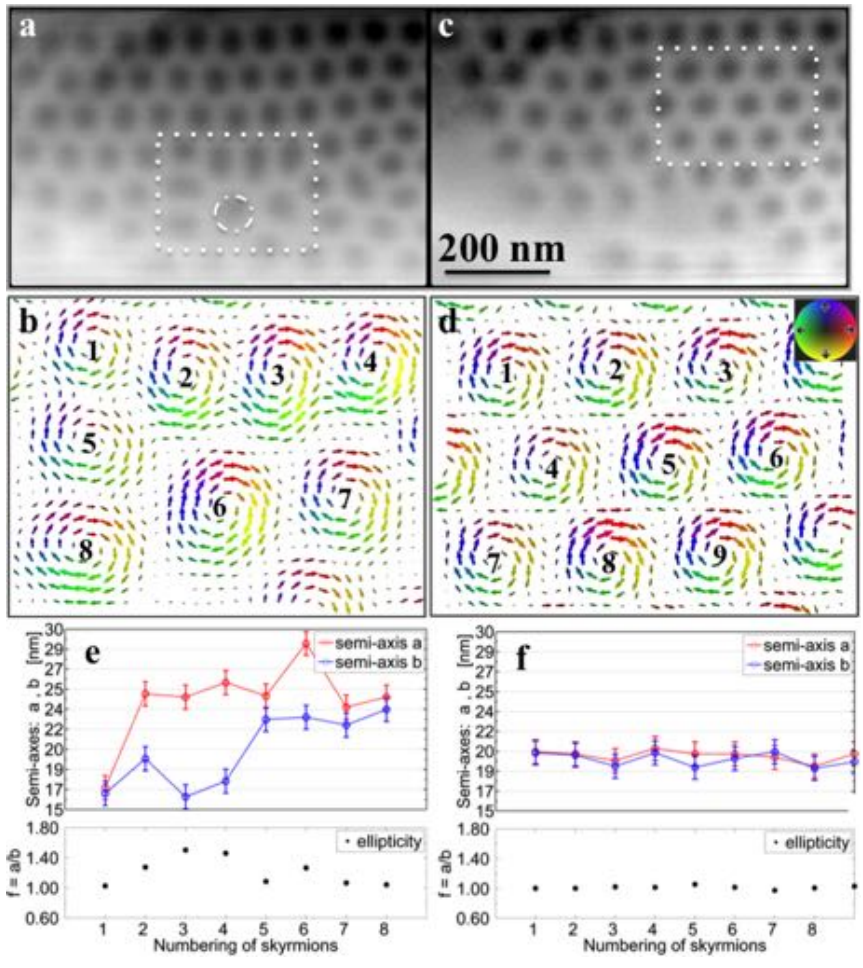

Figure 6. Spin textures of magnetic skyrmion dislocations in an FeGe lamella recorded using off-axis electron holography. (a, c) Magnetic phase images. (b, d) Projected in-plane magnetization corresponding to the areas in panels a and c. The dash-dotted circle in panel a marks the skyrmion dislocation cores. Color wheel is shown as an inset to panel d. (e, f) Experimentally measured values of semiaxes a and b and their ellipticity (defined as $f = a/b$) of ellipse determined from the skyrmions as numbered in panels b and d, respectively.

ization at the grain boundaries reveals that the skyrmions form on both sides of the grains at the very boundary. The close-packed skyrmions to the boundary can be attributed to the weak DM interactions relative to the strong exchange interaction in FeGe with a helical period of about 70 nm. Thus, skyrmion spin structures in FeGe are less affected by changes of the short-range across the atomically sharp boundaries with identical magnetic chirality.

Lorentz Microscopy of Skyrmion Dislocation. We now illustrate the formation of magnetic skyrmion lattice defects in

DOI: 10.1021/acs.nanolett.6b04280
Nano Lett. 2017, 17, 1395−1401

single grains that contain no grain boundary-type planar defects. Figure 5a shows a bright-field TEM image of a FIB-prepared FeGe nanostripe. Figures 5b and c show Lorentz images of the thin part of the nanostripe marked in Figure 5a. We note that the same in-field (100 mT) cooling procedure was applied but with adjustable cooling rates by electrical heating for the two cases. The cooling rate is about 10 K min^{-1} for Figure 5b (without heating) and about 1 K min^{-1} for Figure 5c. The round contrast features are associated with skyrmion lattice formation at a specimen temperature of 100 K. Figure 5b shows the skyrmion lattice with a dislocation-like defect, while Figure 5c shows a well-ordered eight-row lattice arrangement. Interestingly, magnetic skyrmions in the dislocation core region (indicated by a dashed circle in Figure 5b) have irregular morphologies when compared to the well-ordered skyrmion arrangement shown in Figure 5c. Such morphological irregularities are associated with the high flexibility of skyrmionic spin textures, which can accommodate themselves flexibly to create lattice defects.[17] The formation of skyrmion defects highlights not only the particle-like properties of skyrmions, which behave similarly to atomic lattice defects, but also the nontrivial topological properties of skyrmions, which permit continuous deformations without changing their topological class. Nevertheless, it should be noted that atoms are rigid objects that are bonded electrostatically via electron clouds, while skyrmions are topologically flexible spin textures that are governed by magnetic interactions.[36,37]

Off-Axis Electron Holography of Skyrmion Dislocation. The Lorentz micrographs shown in Figures 5a and c provide direct visualizations of skyrmion lattices with and without magnetic dislocations in an FeGe nanostripe that was subjected to a temperature of 100 K and an applied magnetic field of 100 mT. We again turn to the analysis of magnetic phase image recorded using off-axis EH to determine the projected in-plane magnetization, as described in the Supporting Information. Figures 6a and b show magnetic phase images of skyrmion lattices with and without a dislocation, respectively. The contrast in each image represents the projected in-plane magnetic induction of the skyrmion arrangement. The projected in-plane magnetization distribution was determined from each magnetic phase image by using the magnetization reconstruction technique described above and in the Supporting Information. Figures 6b and d show the reconstructed in-plane magnetization distributions of the regions marked in Figures 6a and c, respectively. Note that only one-fifth of the reconstructed spins are plotted. In Figure 6b, the reconstructed spin texture in the dislocation core region reveals that the skyrmion diameter in the dislocation core is approximately 30% larger than that of a regular skyrmion (~80 nm) and that neighboring skyrmions have smaller sizes and exhibit elliptical distortions. In contrast, the well-ordered skyrmions in Figure 6d have regular sizes and circular morphologies. The deformation of each skyrmion was estimated by fitting an elliptical shape with semiaxes a and b to its magnetic contrast profile obtained using off-axis EH. We describe the ellipticity by defining a parameter $f = a/b$, which is 1 when a skyrmion is circular and deviates from 1 as the projected shape become elliptically distorted. Figures 6e and f show the experimentally determined semiaxes a and b as well as their ellipticity f for the skyrmions in Figures 6b and d, respectively. These data quantitatively show the larger distortions of skyrmions at the dislocation core, as compared to skyrmions in the regular lattices.

Conclusions. We have investigated the spin textures of magnetic skyrmion lattices using in situ Lorentz microscopy and off-axis electron holography, with a particular focus on correlating skyrmion lattice defects with underlying material defects. For skyrmion defects that are mediated by underlying crystallographic grain boundaries, we observed interface spin stripes at grain boundaries, across which the crystallographic and hence magnetic chirality reversed. In the absence of crystallographic defects, we found that individual skyrmions were able to flexibly adapt their sizes and morphologies at skyrmion defects. The skyrmionic lattice defects that we observed are important for the exploitation of skyrmion-based devices, as material imperfections affect the particle-like properties of topologically protected spin textures and are likely to have a strong effect on magnetotransport properties and spin wave excitations in magnetic skyrmion crystals.

■ ASSOCIATED CONTENT

Supporting Information

The Supporting Information is available free of charge on the ACS Publications website at DOI: 10.1021/acs.nanolett.6b04280.

Notes on in situ Lorentz micrsocpy LM and quantitative off-axis electron holography EH; supporting figures for specimen preparation and structural characterization; schematics of LM and EH; procedure of magnetic contrast analysis (PDF)

Video of Lorentz images (AVI)

Video of Lorentz images (AVI)

■ AUTHOR INFORMATION

Corresponding Author

*E-mail: zali79@iphy.ac.cn.

ORCID

Zi-An Li: 0000-0002-6338-8933

Amir Hossein Tavabi: 0000-0003-1551-885X

Notes

The authors declare no competing financial interest.

■ ACKNOWLEDGMENTS

We thank Dr. Nikolai Kiselev for helpful discussions. This work was supported by the Natural Science Foundation of China (Grant Nos. 11474290, 11374302, and U1432251). The research leading to these results has received funding from the European Research Council under the European Union's Seventh Framework Programme (FP7/2007-2013)/ ERC grant agreement number 320832.

■ REFERENCES

(1) Nagaosa, N.; Tokura, Y. *Nat. Nanotechnol.* **2013**, *8*, 899.

(2) Roessler, U. K.; Bogdanov, N.; Pfleiderer, C. *Nature* **2006**, *442*, 797.

(3) Jonietz, F.; Mühlbauer, S.; Pfleiderer, C.; Neubauer, A.; Munzer, W.; Bauer, A.; Adams, T.; Georgii, R.; Boni, P.; Duine, R. A.; Everschor, K.; Garst, M.; Rosch, A. *Science* **2010**, *330*, 1648.

(4) Iwasaki, J.; Mochizuki, M.; Nagaosa, N. *Nat. Commun.* **2013**, *4*, 1463.

(5) Fert, A.; Cros, V.; Sampaio, J. *Nat. Nanotechnol.* **2013**, *8*, 152.

(6) Dzyaloshinsky, I. *J. Phys. Chem. Solids* **1958**, *4*, 241.

(7) Moriya, T. *Phys. Rev.* **1960**, *120*, 91.

(8) Mühlbauer, S.; Binz, B.; Jonietz, F.; Pfleiderer, C.; Rosch, A.; Neubauer, A.; Georgii, R.; Boni, P. *Science* **2009**, *323*, 915−919.

DOI: 10.1021/acs.nanolett.6b04280
Nano Lett. 2017, 17, 1395−1401

(9) Yu, X. Z.; Onose, Y.; Kanazawa, N.; Park, J. H.; Han, J. H.; Matsui, Y.; Nagaosa, N.; Tokura, Y. *Nature* **2010**, *465*, 901.
(10) Yu, X. Z.; Kanazawa, N.; Onose, Y.; Kimoto, K.; Zhang, W. Z.; Ishiwata, S.; Matsui, Y.; Tokura, Y. *Nat. Mater.* **2011**, *10*, 106.
(11) Heinze, S.; von Bergmann, K.; Menzel, M.; Brede, J.; Kubetzka, A.; Wiesendanger, R.; Bihlmayer, G.; Bluegel, S. *Nat. Phys.* **2011**, *7*, 713−718.
(12) Woo, S. H.; et al. *Nat. Mater.* **2016**, *15*, 501−507.
(13) Milde, P.; Koehler, D.; Seidel, J.; Eng, L. M.; Bauer, A.; Chacon, A.; Kindervater, J.; Muhlbauer, S.; Pfleiderer, C.; Buhrandt, S.; Schutte, C.; Rosch, A. *Science* **2013**, *340*, 1076−1080.
(14) Uchida, M.; Nagaosa, N.; He, J. P.; Kaneko, Y.; Iguchi, S.; Matsui, Y.; Tokura, Y. *Phys. Rev. B: Condens. Matter Mater. Phys.* **2008**, *77*, 184402−184406.
(15) Park, H. S.; Yu, X. Z.; Aizawa, S.; Tanigaki, T.; Akashi, T.; Takahashi, Y.; Matsuda, T.; Kanazawa, N.; Onose, Y.; Shindo, D.; Tonomura, A.; Tokura, Y. *Nat. Nanotechnol.* **2014**, *9*, 337−342.
(16) Shibata, K.; Kovacs, A.; Kanazawa, N.; Dunin-Borkowski, R. E.; Tokura, Y. *arXiv:1606.05723v1*. **2016**.
(17) Matsumoto, T.; So, Y.-G.; Kohno, Y.; Sawada, H.; Ikuhara, Y.; Shibata, N. *Sci. Adv.* **2016**, *2*, e1501280−e1501284.
(18) McGrouther, D.; Lamb, R. J.; Krajnak, M.; McFadzean, S.; McVitie, S.; Stamps, R. L.; Leonov, A. O.; Bogdanov, A. N.; Togawa, Y. *New J. Phys.* **2016**, *18*, 095004−095015.
(19) Tonomura, A.; Yu, X.; Yanagisawa, K.; Matsuda, T.; Onose, Y.; Kanazawa, N.; Park, H. S.; Tokura, Y. *Nano Lett.* **2012**, *12*, 1673−1677.
(20) Nagao, M.; So, Y. G.; Yoshida, H.; Nagai, T.; Edagawa, K.; Saito, K.; Hara, T.; Yamazaki, A.; Kimoto, K. *Appl. Phys. Express* **2015**, *8*, 033001−033004.
(21) Nagao, M.; So, Y. G.; Yoshida, H.; Yamaura, K.; Nagai, T.; Hara, T.; Yamazaki, A.; Kimoto, K. *Phys. Rev. B: Condens. Matter Mater. Phys.* **2015**, *92*, 140415R.
(22) Yu, X. Z.; Kikkawa, A.; Morikawa, D.; Shibata, K.; Tokunaga, Y.; Taguchi, Y.; Tokura, Y. *Phys. Rev. B: Condens. Matter Mater. Phys.* **2015**, *91*, 054411−054417.
(23) Dunin-Borkowski, R. E.; Kasama, T.; Beleggia, M.; Pozzi, G. *Lorentz Microscopy and Electron Holography of Magnetic Materials*; Van Tendeloo, G., Van Dyck, D., Pennycook, S. J., Eds.; WILEY-VCH GmbH & Co. KGaA, 2012; Chapter 6.
(24) Du, H.; Che, R.; Kong, L. Y.; Zhao, X.; Jin, C. M.; Wang, C.; Yang, J. Y.; Ning, W.; Li, R.; Jin, C. Q.; Chen, X.; Zang, J.; Zhang, Y.; Tian, M. *Nat. Commun.* **2015**, *6*, 8504−8508.
(25) Glazer, A. M.; Stadnicka, K. *J. Appl. Crystallogr.* **1986**, *19*, 108−122.
(26) Ishida, M.; Endoh, Y.; Mitsuda, S.; et al. *J. Phys. Soc. Jpn.* **1985**, *54*, 2975−2982.
(27) Tanaka, M.; Takayoshi, H.; Ishida, M.; Endoh, Y. *J. Phys. Soc. Jpn.* **1985**, *54*, 2970−2974.
(28) *International Tables for Crystallography*, 5th ed.;Hahn, T., Ed.; The International Union Of Crystallography, Springer, 2005; Vol. *A*.
(29) Grigoriev, S. V.; Chernyshov, D.; Dyadkin, V. A.; Dmitriev, V.; Maleyev, S. V.; Moskvin, E. V.; Menzel, D.; Schoenes, J.; Eckerlebe, H. *Phys. Rev. Lett.* **2009**, *102*, 037204−037207.
(30) Morikawa, D.; Shibata, K.; Kanazawa, N.; Yu, X. Z.; Tokura, Y. *Phys. Rev. B: Condens. Matter Mater. Phys.* **2013**, *88*, 024408−024412.
(31) Rohart, S.; Thiaville, A. *Phys. Rev. B: Condens. Matter Mater. Phys.* **2013**, *88*, 184422−184429.
(32) Rajeswari, J.; Huang, P.; Mancini, G. F.; Murooka, Y.; Latychevskaia, T.; McGrouther, D.; Cantoni, M.; Baldini, E.; White, J. S.; Magrez, A.; Giamarchi, T.; Ronnow, H. M.; Carbone, F. *Proc. Natl. Acad. Sci. U. S. A.* **2015**, *112*, 14212−14217.
(33) Shibata, K.; Yu, X. Z.; Hara, T.; Morikawa, D.; Kanazawa, N.; Kimoto, K.; Ishiwata, S.; Matsui, Y.; Tokura, Y. *Nat. Nanotechnol.* **2013**, *8*, 723−728.
(34) Lichte, H.; Lehmann, M. *Rep. Prog. Phys.* **2008**, *71*, 016102.
(35) Lebech, B.; Bernhard, J.; Freltoft, T. *J. Phys.: Condens. Matter* **1989**, *1*, 6105−6122.
(36) Bogdanov, A. N.; Yablonskii, D. A. *Sov. Phys. JETP.* **1989**, *68*, 101.
(37) Bogdanov, A. N.; Hubert, A. *J. Magn. Magn. Mater.* **1994**, *138*, 255.

DOI: 10.1021/acs.nanolett.6b04280
Nano Lett. 2017, 17, 1395−1401